ANALYSIS OF EMITTANCE GROWTH IN A GRIDLESS SPECTRAL POISSON SOLVER FOR FULLY SYMPLECTIC MULTIPARTICLE TRACKING

C. E. Mitchell*, Ji Qiang, Lawrence Berkeley National Laboratory, Berkeley, CA 94720, USA

Abstract

Gridless spectral methods for self-consistent symplectic space charge modeling possess several advantages over traditional momentum-conserving particle-in-cell methods, including the absence of numerical grid heating and the presence of an underlying multi-particle Hamiltonian. Nevertheless, evidence of collisional particle noise remains. For a class of such 1D and 2D algorithms, we provide analytical models of the numerical field error, the optimal choice of spectral modes, and the numerical emittance growth per time step. We compare these results with the emittance growth models of Struckmeier, Hoffman, Kesting, and others.

INTRODUCTION

Distinguishing between physical and numerical emittance growth observed in long-term tracking of beams with space charge is critical to understanding beam performance in high-intensity proton rings. Numerical emittance growth has been modeled as a collisional increase of the beam phase space volume driven by random noise caused by the use of a small number of macroparticles [1–4]. Recently, several authors have developed methods for multiparticle tracking (in plasmas or beams) using variational or explicitly symplectic algorithms designed to preserve the geometric properties of the self-consistent equations of motion [5–7]. In this paper, we address the problem of numerical emittance growth generated by the multi-particle symplectic algorithm described in [7]. Due to its relative simplicity, this algorithm can be used as a test-bed for explicit probabilistic models of numerical errors in the computed field and numerical emittance growth.

SYMPLECTIC SPECTRAL ALGORITHM

We apply the algorithm described in Section III of [7] to treat the Poisson equation in a general bounded domain $\Omega \subset \mathbb{R}^d$ ($d \leq 2$) with conducting boundary $\partial\Omega$. The symplectic map describing a numerical step in the path length coordinate s is performed by applying second-order operator splitting to the following multi-particle Hamiltonian:

$$H = \sum_{j=1}^{N_p} H_{\text{ext}}(\vec{r}_j, \vec{p}_j, s) - \frac{n}{N_p}\frac{1}{2}\sum_{j=1}^{N_p}\sum_{k=1}^{N_p}\sum_{l=1}^{N_l}\frac{1}{\lambda_l}e_l(\vec{r}_j)e_l(\vec{r}_k).$$

Here H_{ext} is the single-particle Hamiltonian in the external applied fields, N_p denotes the number of simulation particles, N_l denotes the number of computed modes, and n is a space charge intensity parameter. The smooth functions e_l

---

* ChadMitchell@lbl.gov

form an orthonormal basis for the space of square-integrable functions on the domain Ω, and satisfy

$$\nabla^2 e_l = \lambda_l e_l, \quad e_l|_{\partial\Omega} = 0, \quad (\lambda_l < 0). \quad (1)$$

It follows from H that each particle moves in response to the smooth space charge force $\vec{F} = -\nabla U$, where

$$U(\vec{r}) = -\frac{n}{N_p}\sum_{l=1}^{N_l}\sum_{j=1}^{N_p}\frac{1}{\lambda_l}e_l(\vec{r}_j)e_l(\vec{r}). \quad (2)$$

The space charge potential U satisfies the Poisson equation $\nabla^2 U = -\rho$ and $U|_{\partial\Omega} = 0$, where ρ is a particle-based approximation to the beam density, given in terms of the modes e_l ($l = 1, 2, \ldots$) by:

$$\rho = \sum_{l=1}^{N_l}\rho^l e_l, \quad \rho^l = \frac{n}{N_p}\sum_{j=1}^{N_p}e_l(\vec{r}_j). \quad (3)$$

The set of functions

$$\vec{e}_l = \frac{1}{\sqrt{-\lambda_l}}\nabla e_l \quad (l = 1, 2, \ldots) \quad (4)$$

is orthonormal and can be extended to an orthonormal basis for the space of square-integrable vector-valued functions on Ω. The relationships between the corresponding modes of ρ, U, and $\vec{F}$ are then given simply by:

$$U^l = \rho^l/\lambda_l, \quad F^l = -\sqrt{-\lambda_l}U^l. \quad (5)$$

By appropriately grouping the sums appearing in the space charge kick, the complexity of a single numerical step using the Hamiltonian H scales as $O(N_p N_l)$ [7].

PROBABILISTIC MODEL

Assume that particle coordinates $(\vec{r}_j, \vec{p}_j)$, $j = 1, \ldots, N_p$ are sampled from the joint probability density P_N given by:

$$P_N(\vec{r}_1, \vec{p}_1, \ldots, \vec{r}_{N_p}, \vec{p}_{N_p}) = \prod_{j=1}^{N_p}P(\vec{r}_j, \vec{p}_j), \quad (6)$$

where P is the probability density on the single-particle phase space describing an ideal (smooth) beam distribution. If a denotes any function on the single-particle phase space, we denote its beam-based average by

$$\langle a \rangle = \frac{1}{N_p}\sum_{j=1}^{N_p}a(\vec{r}_j, \vec{p}_j), \quad \Delta a = a - \langle a \rangle. \quad (7)$$

Likewise, if F, G denote random variables on the multi-particle phase space, we denote their expected value and covariance as

$$E[F] = \int F dP_N, \quad Cov[F, G] = E[FG] - E[F] E[G].$$

If a_1 and a_2 denote two functions on the single-particle phase space, then $\langle a_1 \rangle$ and $\langle a_2 \rangle$ define random variables on the multi-particle phase space, and it follows from the fact that distinct particles are independent and identically distributed, see Eq. (6), that ($j = 1, 2$)

$$E[\langle a_j \rangle] = E[a_j], \quad Cov[\langle a_1 \rangle, \langle a_2 \rangle] = \frac{1}{N_p} Cov[a_1, a_2].$$

A generalization of this result is provided in the Appendix.

FIELD ERROR AND OPTIMAL MODES

Field Error

The space charge potential of an ideal beam with density ρ_{exact} is given by the exact solution of the Poisson equation:

$$\nabla^2 U_{exact} = -\rho_{exact}, \quad U_{exact}|_{\partial\Omega} = 0, \quad (8)$$

where ρ_{exact} is the spatial projection of the phase space density nP appearing in Eq. (6). It follows that

$$\rho_{exact}^l = \int_\Omega \rho_{exact}(\vec{r}) e_l(\vec{r}) d\vec{r} = n E[e_l]. \quad (9)$$

Let $\delta\rho = \rho - \rho_{exact}$ and $\delta\vec{F} = \vec{F} - \vec{F}_{exact}$, where ρ and $\vec{F}$ are the numerically computed quantities obtained using Eqs. (2–5). It follows that for all modes with $l, m \leq N_l$,

$$E[\delta\rho^l] = 0, \quad Cov[\delta\rho^l, \delta\rho^m] = \frac{n^2}{N_p} Cov[e_l, e_m]. \quad (10)$$

Using the relationships in Eq. (5) gives:

$$E[\delta F^l \delta F^m] = \begin{cases} \frac{1}{N_p} \frac{n^2}{\sqrt{\lambda_l \lambda_m}} Cov[e_l, e_m] & (l, m \leq N_l) \\ \frac{n^2}{\sqrt{\lambda_l \lambda_m}} E[e_l] E[e_m] & (l, m > N_l) \end{cases}. \quad (11)$$

The mean-squared value of the computed field error at any point $\vec{r} \in \Omega$ is then given by:

$$E[|\delta\vec{F}(\vec{r})|^2] = \sum_{l,m=1}^\infty E[\delta F^l \delta F^m] \vec{e}_l(\vec{r}) \cdot \vec{e}_m(\vec{r}). \quad (12)$$

Define the L^2 norm of the error in the computed field by:

$$||\delta\vec{F}||^2 = \int_\Omega |\delta\vec{F}(\vec{r})|^2 d\vec{r} = \sum_{l=1}^\infty \left(\delta F^l\right)^2. \quad (13)$$

Taking the expected value of Eq. (13) using Eq. (11) gives:

$$E[||\delta\vec{F}||^2] = -\frac{1}{N_p} \sum_{l=1}^{N_l} \frac{n^2}{\lambda_l} Var[e_l] - \sum_{l=N_l+1}^\infty \frac{n^2}{\lambda_l} E[e_l]^2. \quad (14)$$

The quantity Eq. (14) splits cleanly into contributions due to particle noise (leftmost sum) and mode truncation (rightmost sum).

Numerical 1D Example

Consider a 1D domain $\Omega = (0, a)$ containing a beam with an ideal beam distribution P with parabolic spatial profile:

$$P(x, p) = \frac{3}{4h} \left\{ 1 - \frac{(x-d)^2}{h^2} \right\} \delta(p), \quad |x - d| \leq h. \quad (15)$$

Figure 1 illustrates the predicted rms error in the computed field (black), together with the statistically computed rms error obtained by averaging over 200 distinct random seeds (red dashed). We see good agreement with the analytical model Eqs. (11–12). The error is largest near the beam core, with Gibbs ringing near the beam edges. Figure 2
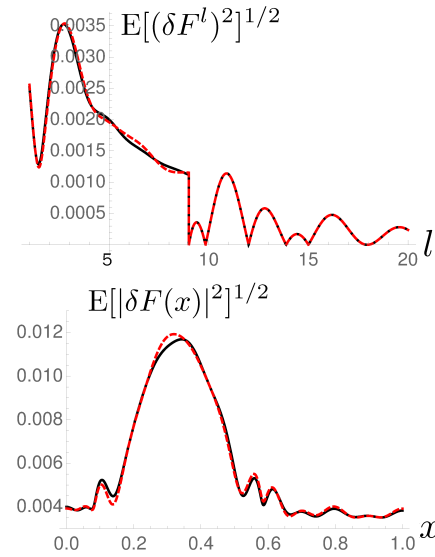
Figure 1: Error in the computed field obtained using $N_p = 1000$, $N_l = 9$, $n = 1$ corresponding to the density Eq. (15) with $a = 1$, $d = 1/3$, and $h = 1/4$. (Upper) RMS error in the coefficient of mode l. (Lower) RMS error in the field at each position x.

illustrates the expected norm of the field error as a function of the number of particles and the number of modes. For fixed $N_l = 9$, the error decreases monotonically with N_p, approaching a nonzero limit. However, for fixed $N_p = 1000$, the error attains a minimum near $N_l = 9$. The problem of choosing an optimal mode cutoff is addressed in the next section.

Optimal Mode Set

For an ideal density ρ_{exact}, we can determine the optimal set of modes S that must be computed to minimize the expected total error Eq. (14). Since $\lambda_l < 0$, every term in this sum is nonnegative. Since every mode with index l must contribute to either the leftmost sum or the rightmost sum in Eq. (14), the quantity Eq. (14) is globally minimized when we enforce the condition that $l \in S$ if and only if:

$$\frac{E[(\delta F^l)^2]}{(F_{exact}^l)^2} = \frac{Var[\delta\rho^l]}{(\rho_{exact}^l)^2} = \frac{1}{N_p} \frac{Var[e_l]}{E[e_l]^2} \leq 1. \quad (16)$$
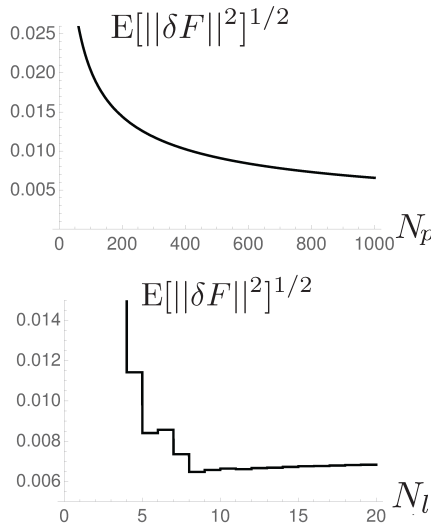
Figure 2: Norm of the error in the computed field corresponding to the beam density Eq. (15) with $a = 1$, $d = 1/3$, and $h = 1/4$. (Upper) Shown vs. number of particles for fixed mode cutoff $N_l = 9$. (Lower) Shown vs. number of modes for fixed $N_p = 1000$. In both cases $n = 1$.

That is, $l \in S$ if and only if the rms size of fluctuations in the coefficient ρ^l resulting from particle noise is less than or equal to the value of ρ^l for the ideal (smooth) density. Because $E[e_l]^2$ generally decays more rapidly that $Var[e_l]$ with increasing index l, the set S is generally finite, and it follows from Eq. (16) that the optimal number of modes increases monotonically with the number of simulation particles N_p. Note that even in 1D, the optimal set S does not in general take the form of a consecutive set of indices $S = \{1, 2, 3, \ldots, N_l\}$.

ANALYSIS OF EMITTANCE GROWTH

Emittance Growth on a Single Step

Consider the case of a beam propagating with space charge in a set of linear external focusing fields. The change in x-emittance under a space charge kick $(x, p) \mapsto (x, p + \tau F)$ of step size τ is given by:

$$\epsilon^2 - \epsilon_0^2 = 2\tau A + \tau^2 B, \tag{17}$$

where the terms A and B take the forms:

$$A = \langle \Delta x^2 \rangle \langle \Delta p \Delta F \rangle - \langle \Delta x \Delta p \rangle \langle \Delta x \Delta F \rangle, \tag{18}$$

$$B = \langle \Delta x^2 \rangle \langle \Delta F^2 \rangle - \langle \Delta x \Delta F \rangle^2. \tag{19}$$

Note that Eq. (18) may have variable sign, while Eq. (19) is always nonnegative. Both A and B are invariant under the transformation:

$$x \to x + c, \quad p \to p + ax + b, \quad F \to F + gx + h \tag{20}$$

for any constants a, b, c, g, and h. This allows us to remove all linear correlations with x, writing

$$x = E[x] + x_u, \tag{21}$$

$$p = E[p] + \frac{Cov[x, p]}{Var[x]}(x - E[x]) + p_u, \tag{22}$$

$$e_l' = E[e_l'] + \frac{Cov[x, e_l']}{Var[x]}(x - E[x]) + e_{l,u}'. \tag{23}$$

Here $e_l' = \partial e_l / \partial x$. Replacing x, p, and e_l' with x_u, p_u, and $e_{l,u}'$ if necessary, we may therefore assume that $E[x] = 0$, $E[p] = 0$, $E[e_l'] = 0$, $Cov[x, p] = 0$, and $Cov[x, e_l'] = 0$. Applying our probabilistic model to the random variables A and B using the results of the Appendix gives a decomposition into modes of the form:

$$E[A] = \sum_{l=1}^{N_l} \frac{n}{\lambda_l} A^l, \quad E[B] = \sum_{l,m=1}^{N_l} \frac{n^2}{\lambda_l \lambda_m} B^{lm}, \tag{24}$$

$$Var[A] = \sum_{l,m=1}^{N_l} \frac{n^2}{\lambda_l \lambda_m} A^{lm}, \tag{25}$$

$$Var[B] = \sum_{l,m,l',m'=1}^{N_l} \frac{n^4}{\lambda_l \lambda_m \lambda_{l'} \lambda_{m'}} B^{lml'm'}. \tag{26}$$

In general, the mode coefficients are complicated and must be evaluated using computer algebra. However, in the smooth beam limit $N_p \to \infty$, we have:

$$\lim_{N_p \to \infty} A^l = Var[x] Cov[p, e_l'] E[e_l], \tag{27}$$

$$\lim_{N_p \to \infty} B^{lm} = Var[x] Cov[e_l', e_m'] E[e_l] E[e_m]. \tag{28}$$

Note also that $Var[A]$ and $Var[B]$ are each $O(1/N_p)$. If P is chosen such that x and p are independent (aside from possible linear correlation), we also have the following results, accurate through first order in $1/N_p$:

$$E[A] = 0, \quad Var[A] = \frac{1}{N_p} Var[x] Var[p] E[B]. \tag{29}$$

Finally, we may evaluate the coefficients appearing in $E[B]$ through first order in $1/N_p$ to give:

$$B^{lm} = \lim_{N_p \to \infty} B^{lm} + \frac{1}{2N_p}(T^{lm} + T^{ml}), \tag{30}$$

where

$$\begin{aligned}
T^{lm} = & \; Var[x] Cov[e_l', e_m'] Cov[e_l, e_m] \\
& - 3 Var[x] Cov[e_l', e_m'] E[e_l] E[e_m] \\
& + 2 Cov[x^2, e_l] Cov[e_l', e_m'] E[e_m] \\
& + 2 Var[x] Cov[e_l' e_m', e_l] E[e_m].
\end{aligned} \tag{31}$$

These results can be compared to the model of emittance growth on a single step described in Section IV of [4]. That model is equivalent to treating the kick F as a random field

13th Int. Computational Accelerator Physics Conf.　　ICAP2018, Key West, FL, USA　　JACoW Publishing

ISBN: 978-3-95450-200-4　　　　　　　　　　　　　　doi:10.18429/JACoW-ICAP2018-WEPLG01

with $E[F(x)] = 0$ and spatially-varying $\mathrm{Var}[F(x)]$, and neglecting contributions to the emittance due to statistical fluctuations in the beam moments and nonlinear correlations between F and x. Applying this model to Eq. (18–19) gives:

$$E[A] = 0, \quad E[B] = \mathrm{Var}[x]\, E[\mathrm{Var}[F(x)]]. \quad (32)$$

Using the model of numerical field error given in the previous section Eq. (12), we find (in the 1D case) that:

$$\mathrm{Var}[F(x)] = \frac{1}{N_p} \sum_{l,m=1}^{N_l} \frac{n^2}{\lambda_l \lambda_m} \mathrm{Cov}[e_l, e_m] e'_l(x) e'_m(x). \quad (33)$$

It follows from Eq. (33) that

$$E[B] = \frac{1}{N_p} \sum_{l,m=1}^{N_l} \frac{n^2}{\lambda_l \lambda_m} \mathrm{Var}[x]\, \mathrm{Cov}[e_l, e_m]\, \mathrm{Cov}[e'_l, e'_m]. \quad (34)$$

Comparing with Eq. (31), we see that this approximation is equivalent to assuming that the emittance growth vanishes in the limit $N_p \to \infty$ and neglecting all but the first term of Eq. (31).

Numerical 1D Example

Consider a 1D domain $\Omega = (0, a)$, using an ideal beam distribution P of the form:

$$P(x, p) = \frac{1}{2\pi \sigma_p \sigma_x} \exp\left(-\frac{p^2}{2\sigma_p^2}\right) \exp\left(-\frac{(x - a/2)^2}{2\sigma_x^2}\right). \quad (35)$$

A statistical test was performed as follows. We randomly generated a beam consisting of N_p particles (x, p) by sampling from the density Eq. (35). The space charge force $F(x)$ was computed at all particle locations using the symplectic spectral algorithm with $N_l = 15$, $n = 1$. Terms A and B of Eqs. (18–19) were computed, and this procedure was repeated for 1M distinct random seeds. Fig. 3 provides histograms of the results, illustrating the probability density of the random variables A and B. In each figure, the quantity on the horizontal axis is shown after subtracting the expected value obtained in the smooth beam limit $N_p \to \infty$, given by using Eqs. (27–28) in Eq. (24). Here $\lim_{N_p \to \infty} E[A] = 0$ and $\lim_{N_p \to \infty} E[B] = 3.75 \times 10^{-3}$. The results become more sharply peaked around the predicted smooth limiting value as $N_p \to \infty$, with a standard deviation that scales as $O(1/\sqrt{N_p})$, as predicted. Table 1 provides the mean and standard deviation of A and B. Comparing the computed mean μ and standard deviation σ of A with the prediction Eq. (29), we see that μ deviates from $E[A]$ by $< 10^{-6}$, and σ is in agreement with $\mathrm{Var}[A]^{1/2}$.

Emittance Growth in a FODO Channel

We modeled a 1 GeV proton beam with 100 A current in a FODO lattice of period 1 m, using a 2D rectangular domain of size 6.5×6.5 mm. The lattice zero current phase advance per period is 87 degrees, and the depressed phase advance is 74 degrees. Figure 4 shows the emittance evolution of
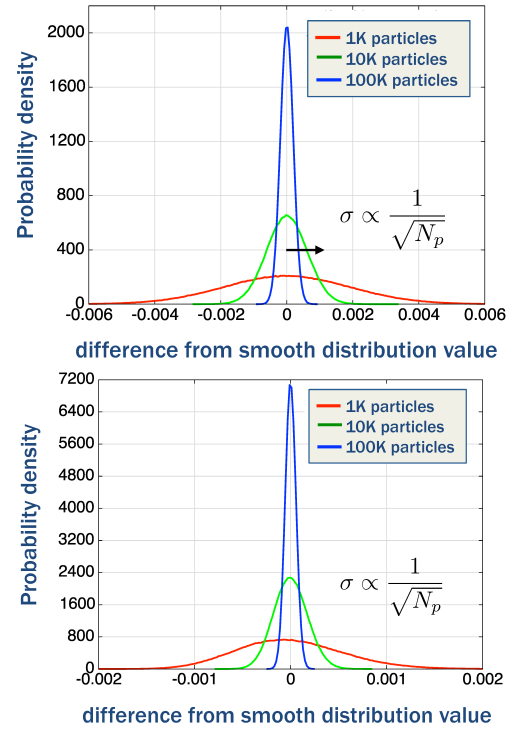
Figure 3: Probability density for the emittance contributions A and B of Eqs. (18–19) for the case $N_l = 15$, $n = 1$, obtained by sampling beams with varying N_p using 1M random seeds. (Upper) Term A. (Lower) Term B. The values of A and B are statistically uncorrelated.

Table 1: Emittance Contributions on a Single Step

	term A		term B	
N_p	μ	σ	μ	σ
10^3	-9.9×10^{-7}	1.9×10^{-3}	2.2×10^{-6}	5.5×10^{-4}
10^4	-3.3×10^{-7}	6.1×10^{-4}	4.1×10^{-7}	1.8×10^{-4}
10^5	$+2.9 \times 10^{-7}$	1.9×10^{-4}	1.0×10^{-7}	5.6×10^{-5}

an initially matched KV beam with $\epsilon_{x,n} = \epsilon_{y,n} = 1\ \mu m$ over 100,000 periods using 15 horizontal and 15 vertical modes (so $N_l = 15 \times 15$). Despite the small number of modes and the small number of particles, the emittance is preserved within 0.4%. The emittance evolution is dominated by period-period fluctuations, and the rms amplitude of these fluctuations scales as $N_p^{-\beta}$, with a best fit exponent of $\beta = 0.57$, approximately consistent with $O(1/\sqrt{N_p})$.

By contrast, Fig. 5 shows the emittance evolution of an initially matched Gaussian beam with $\epsilon_{x,n} = \epsilon_{y,n} = 1\ \mu m$ using 32×32 modes, illustrating linear emittance growth. A least-squares fit to determine the emittance growth rate was performed for each value of N_p, and the resulting emittance growth rate data scales as $N_p^{-\alpha}$ with $\alpha = 0.996$, consistent with $O(1/N_p)$. The rms amplitude of residual fluctuations after removing the linear fit indicates that these fluctuations

scale as $N_p^{-\beta}$, with $\beta = 0.58$, similar to the KV case and nearly consistent with $O(1/\sqrt{N_p})$.
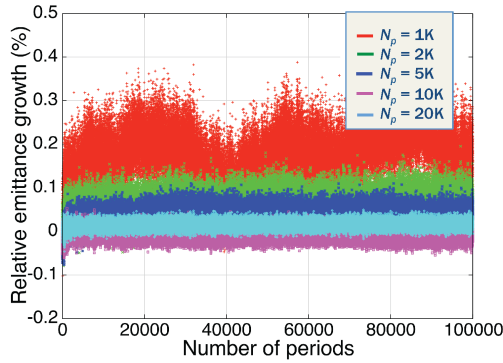
Figure 4: Evolution of the 4D emittance $\sqrt{\epsilon_x \epsilon_y}$ for a matched KV beam propagating in a FODO lattice using 15×15 spectral modes for several values of N_p.
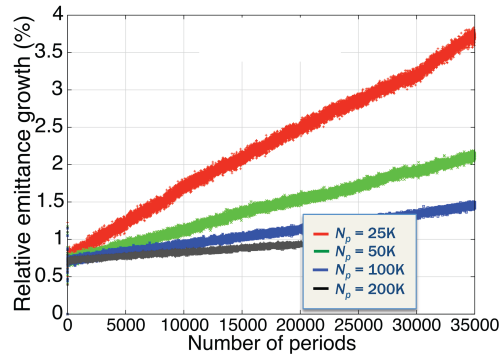
Figure 5: Evolution of the 4D emittance $\sqrt{\epsilon_x \epsilon_y}$ for an initially Gaussian beam propagating in the same FODO lattice using 32×32 spectral modes for several values of N_p.

Letting ϵ_n denote the emittance after the nth numerical step, we have the expected emittance change at step n:

$$\mathrm{E}[\epsilon_n^2 - \epsilon_{n-1}^2] = 2\tau \, \mathrm{E}[A] + \tau^2 \, \mathrm{E}[B], \tag{36}$$

where A and B denote the contributions Eqs. (18–19) at step n. Dividing by τ, assuming that the ideal (smooth) beam distribution evolves slowly from step to step (a questionable assumption), and assuming a relative emittance growth $<<$ 1, we obtain an approximate expression for the emittance growth rate given by (compare the result in [4]):

$$\mathrm{E}\left[\frac{d\epsilon}{d\tau}\right] \approx \frac{1}{2\epsilon_0} \tau \, \mathrm{E}[B]. \tag{37}$$

Similarly, noting that:

$$\mathrm{Var}[\epsilon_n^2 - \epsilon_{n-1}^2] = 4\tau^2 \, \mathrm{Var}[A] + 4\tau^3 \, \mathrm{Cov}[A, B] + \tau^4 \, \mathrm{Var}[B],$$

keeping to leading order in the stepsize τ, and making the same assumptions as above gives an approximate expression for the rms fluctuations of the emittance from step to step:

$$\sigma_{\Delta\epsilon} \approx \frac{\tau}{\epsilon_0} \mathrm{Var}[A]^{1/2}. \tag{38}$$

Using Eqs. (29) and (34), we see that the two quantities Eqs. (37) and (38) are expected to scale as $O(1/N_p)$ and $O(1/\sqrt{N_p})$, respectively, as observed.

The approximate scaling analysis above effectively neglects horizontal-vertical coupling. A probabilistic treatment of the dynamical emittance growth driven by particle noise in the presence of space charge was previously proposed using a moment analysis of the Vlasov-Fokker-Planck equation [1], [8], where the role of collisional heat exchange between the degrees of freedom is emphasized. A connection could be made by relating the friction and diffusion coefficients in this model to the explicit model of field and single-step emittance growth described here.

CONCLUSION

We developed probabilistic models of the computed field error and numerical emittance growth on a single step for a fully symplectic spectral space charge tracking algorithm [7]. The models described here are independent of the detailed geometry of the domain, which appears indirectly through the set of modes e_l and eigenvalues λ_l. The model of the computed field error, including both particle noise and errors due to the use of a finite mode cutoff, is relatively simple, and can be used to select an optimal set of computed modes that minimizes the expected norm of the computed field error for a given particle number.

A complete probabilistic model of dynamical emittance growth is difficult, but insight can be drawn from a model of emittance growth on a single numerical step. This emittance growth is driven by the two terms Eqs. (18) and (19). Term A in general has negligible expected value, but $\mathrm{Var}[A] \sim O(1/N_p)$, and this variance drives fluctuations in the emittance from step to step, which scale approximately as $O(1/\sqrt{N_p})$. Term B is always nonnegative. Its expected value contains a term that is independent of N_p, which drives emittance growth in the smooth-beam limit, and a term due to particle noise, that drives additional emittance growth scaling as $\sim O(1/N_p)$. Statistical moments of these terms can be decomposed into contributions from various modes, and evaluated for a given beam distribution function. We observe a scaling of emittance growth rates and emittance fluctuations consistent with this model for a beam propagating in a FODO channel.

Additional work is underway to investigate the validity of this probabilistic model by evaluating the role played by statistical correlations between successive numerical steps. Finally, while it appears that symplecticity alone is insufficient to eliminate the diffusive effects of numerical noise, it is suspected that these effects can be further suppressed by using higher-order particle shapes (such as those described in [6]), which serve to additionally filter high-frequency components of the computed space charge fields. A discussion of this approach and additional strategies for noise filtering in space charge tracking is provided in [9].

ACKNOWLEDGEMENTS

APPENDIX

Let a_j ($j = 1, \ldots, N$) and b_k ($k = 1, \ldots, M$) denote functions defined on the single-particle phase space. Under the probability model Eq. (6), we may evaluate the expected value and variance of any polynomial in the beam averages $\langle a_j \rangle$, $\langle b_k \rangle$. This includes, for example, Eqs. (18–19). It follows from the fact that distinct particles are independent and identically distributed that:

$$
\mathrm{E}\left[\prod_{j=1}^{N} \langle a_j \rangle\right] = \prod_{j=1}^{N} \mathrm{E}[a_j] + \tag{39}
$$

$$
\frac{1}{N_p} \sum_{\substack{j,k=1 \\ j<k}}^{N} \mathrm{Cov}[a_j, a_k] \prod_{\substack{n \neq j \\ n \neq k}}^{N} \mathrm{E}[a_n] + O\left(\frac{1}{N_P^2}\right),
$$

and also:

$$
\mathrm{Cov}\left[\prod_{j=1}^{N} \langle a_j \rangle, \prod_{k=1}^{M} \langle b_k \rangle\right] = \tag{40}
$$

$$
\frac{1}{N_p} \sum_{j=1}^{N} \sum_{k=1}^{M} \prod_{r \neq j}^{N} \mathrm{E}[a_r] \prod_{s \neq k}^{M} \mathrm{E}[b_s] \mathrm{Cov}[a_j, b_k] + O\left(\frac{1}{N_P^2}\right).
$$

Throughout this paper, we evaluate all quantities to first order in $1/N_p$. We may use the linearity of $\mathrm{E}[\cdot]$ and the bilinearity of $\mathrm{Cov}[\cdot, \cdot]$ to extend this result to polynomials in $\langle a_j \rangle$, $\langle b_k \rangle$.

REFERENCES

[1] J. Struckmeier, *Phys. Rev. ST Accel. Beams*, vol. 3, pp. 034202, 2000.

[2] O. Boine-Frankenheim, I. Hofmann, J. Struckmeier, and S. Appel, *Nucl. Instrum. Methods Phys. Res. Sect.* A, vol. 770, pp. 164, 2015.

[3] I. Hofmann and O. Boine-Frankenheim, *Phys. Rev. ST Accel. Beams*, vol. 17, pp. 124201, 2014.

[4] F. Kesting and G. Franchetti, *Phys. Rev. ST Accel. Beams*, vol. 18, pp. 114201, 2015.

[5] B. A. Shadwick, A. B. Stamm, and E. G. Evstatiev, *Physics of Plasmas*, vol. 21, pp. 055708, 2014.

[6] S. D. Webb, *Plasma Phys. Control. Fusion*, vol. 58, pp. 034007, 2016.

[7] Ji Qiang, *Phys. Rev. Accel. Beams*, vol. 20, pp. 014203, 2017.

[8] J. Struckmeier, *Phys. Rev. E*, vol. 5, no. 4, pp. 830, 1996.

[9] Ji Qiang, "Long-term simulation of space-charge effects," submitted to *Nucl. Instrum. and Methods in Phys. Res.* A, 2018.